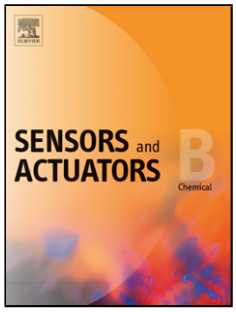

Title: Transparent Polymer-based SERS Substrates Templated by a Soda Can

Authors: Niamh C. Creedon, Pierre Lovera, Ambrose Furey, Alan O'Riordan

PII: S0925-4005(17)32365-1
DOI: https://doi.org/10.1016/j.snb.2017.12.039
Reference: SNB 23727

To appear in: *Sensors and Actuators B*

Received date: 8-9-2017
Revised date: 30-11-2017
Accepted date: 7-12-2017

Please cite this article as: Niamh C.Creedon, Pierre Lovera, Ambrose Furey, Alan O'Riordan, Transparent Polymer-based SERS Substrates Templated by a Soda Can, Sensors and Actuators B: Chemical https://doi.org/10.1016/j.snb.2017.12.039

Transparent Polymer-based SERS Substrates Templated by a Soda Can

Niamh C. Creedon[†], Pierre Lovera[†], Ambrose Furey[§] and Alan O'Riordan[†]*

[†] Department of Nanotechnology, Tyndall National Institute – University College Cork, Lee Maltings, Mardyke Parade, Cork, Ireland

[§] Mass Spectrometry Centre for Proteomics and Biotoxin Research, Department of Chemistry, Cork Institute of Technology, Cork, Ireland.

* Email: alan.oriordan@tyndall.ie

Graphical abstract

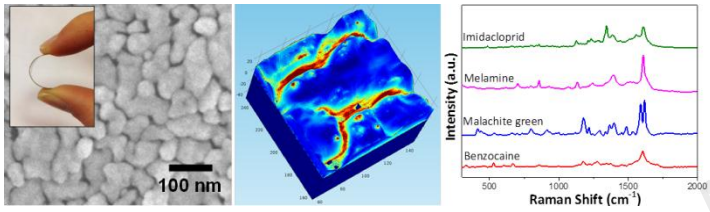

Research Highlights:

- Silver coated transparent flexible polymer substrates (templated with Aluminium soda cans) for use in surface enhanced Raman scattering (SERS) applications.
- The sensors perform very well, exhibiting rapid, quantitative and high sensitivity in 10 minutes using a simple drop and dry method.
- SERS response is also observed via back excitation (the laser impinging on the back of the substrate) with the corresponding spectra exhibiting clear and defined spectral Raman peaks.
- The sensors exhibit sensitive, non-destructive detection of trace amounts of melamine in both milk and infant formula. We show comparable sensitivity between the low-cost SERS substrates and lab based MS-MS.

Abstract

This paper demonstrates the reproducible fabrication of transparent Surface Enhanced Raman Scattering (SERS) substrates, fabricated by employing an aluminium soda can to template nanostructures on a flexible thermoplastic polymer surface,

followed by deposition of a silver over layer. Electron microscopy and finite element modelling simulations strongly suggested the SERS response arose at regions of high electromagnetic field strength occurring between metallic clusters following illumination by monochromatic radiation. The sensors exhibited rapid, quantitative and high sensitivity, for example, 5 x 10^{-10} M (204 pg/mL) crystal violet detection in 10 minutes using a simple drop and dry method. We also show detection of glucose employing a chemically modified silver surface bearing a pre-deposited SAM layer. The transparent substrates permitted back excitation and collection through the substrate which corresponding spectra exhibiting clear and defined spectral SERS peaks. Furthermore, the transparent substrates permitted back excitation and collection through the substrate with corresponding spectra exhibiting clear and defined spectral SERS peaks. Finally, we present the detection of trace amounts of melamine in complex media solution (milk and infant formula). We benchmark the sensor performance using commercial analytical instrumentation (MS-MS) and show comparable sensitivity between the SERS substrates and MS-MS.

Keywords: *Nanostructures, surface enhanced Raman scattering, melamine, mass spectroscopy, metal deposition, templating.*

1. Introduction

In recent years, advances in nanotechnology and nanofabrication techniques have enabled significant enhancement in a variety of analytical sensor devices. These devices, employing electronic [1-3], electrochemical and optical [4-6] detection methods, have provided highly qualitative and sensitive measurements. However, within the environmental and security sectors, highly sensitive sensing alone is not enough; rapid on-site molecular identification is also essential. One analytical approach that addresses these criteria is surface enhanced Raman spectroscopy (SERS) [7, 8] which provides both a spectral molecular fingerprint and allows for trace analyte detection; with the potential for single molecule sensitivity. [9-14] SERS is thus emerging as a powerful technique for remote chemical [15] and biological sensing applications[16].

SERS enhancement occurs at nanostructured plasmonic surfaces following illumination with monochromatic radiation and results from (i) an increase in local electromagnetic field strengths of localised surface plasmons (in nanogaps between metal clusters called “hot spots”) and (ii) chemical resonant energy charge transfer[17-20]. For these processes to occur, substrates must be capable of supporting plasmonic modes (collective oscillations of metal electrons) and have a nanostructured rough surface with well-defined gaps in the region of 10- 100 nm between metallic clusters (to conserve momentum). To this end, fabrication of SERS substrates using top-down approaches including: lithography techniques (Ebeam[21, 22] and nanoimprint[23] lithography’s), laser etching[24], film deposition (sputtering, metal evaporation, atomic layer deposition)[25, 26] and templating (using anodic aluminium oxide [27], masks[25] or molds[28]) as well as bottom-up approaches including chemical synthesis[29], colloid aggregation[30] and self-assembly[31, 32] of metal nanoparticles[33, 34], nanowires[2, 28] , nanospheres[33, 35, 36], nanorods[37-39], nanotubes[27], nanotriangles[40], nano-urchins[41] and/or nanoshells[42] have been reported.

While these approaches are elegant and are attractive in research environments for their large SERS enhancement; they are limited in that they may be expensive, time consuming, and require complex fabrication approaches which may have low throughput. Consequently, a critical challenge inhibiting the uptake of SERS for sensor applications is the lack of scalable, reproducible and fabrication approaches compatible with mass manufacturing. To address this challenge, we have developed a templating approach employing “inherent” nanostructured aluminium (Al) masters (obtained from commercial soda drink cans) to template low-cost polymer replicates which are subsequently coated with a thin (30 nm) silver (Ag) layer. These

transparent polymer substrates offer a number of advantages: (i) the simple manufacturing approach is scalable offering the potential for low-cost fabrication and thus widespread uptake and applicability. (ii) The fine metallic nanostructures provide SERS hot spots upon optical excitation. (iii) The substrates are transparent and thus are compatible with back excitation and collection allowing measurement in liquid environments to be undertaken. ((iv) the flexible substrates may be easily integrated in-line or on-line adding to the suite of spectroscopic process analytical techniques used in smart manufacturing 4.0 approaches. (v) Finally, the sensor may be chemically modified to widen the range of molecules that may be detected.

To explore the versatility of our as-fabricated SERS substrates towards real world applications, e.g., environmental monitoring and food security, a variety of different target molecules were selected and analysed. Initially, 4-aminothiophenol (4-ABT) and crystal violet (CV)[43] were selected to characterise SERS effect and allow comparison with the published literature. We show highly sensitive detection of crystal violet with a measured limit of detection of 204 ng/L (204 parts per trillion, equivalent to 5×10^{-10} M). Malachite green was also selected as this and other trimethyldiamine dyes are used indiscriminately as antimicrobials in aquaculture, despite the reports of causing serious toxic, carcinogenic and mutagenic effects in mammalian cells.[44, 45] Consequently, the presence of trimethyldiamines are now tightly controlled with (MRL) set at 2 µg/L (2 ppb) in water[46]. Glucose was analysed by first capturing the molecule on a substrate pre-modified with a mixed thiol monolayer in a manner similar to that reported by the Van Duyne group [47]. Finally, melamine was selected as it now requires regular monitoring due to its previous use to give a false appearance of high protein levels in milk. [48] Melamine MRLs are now set at 2.5 ppm for food products (including milk) and 1 ppm in infant formulae.[49] We demonstrate detection of low concentrations of melamine (100 ppb) spiked into both milk and infant formula solutions (without sample pretreatment), using a drop-and-dry sampling technique with a total analysis time of 10 minutes and benchmark these results using mass spectroscopy (MS-MS).

2. Material and Methods

2.1. Material and Reagents

Polystyrene (PS), 4-aminothiphenol (97%), polyvinylidene fluoride (PVDF), crystal violet (<90% dye content), malachite green, benzocaine, 1-decanethiol, mercaptohexanol, glucose and melamine and analytical grade solvents were purchased from Sigma-Aldrich (Dublin) and used as received. Polydimethylsiloxane 184 silicon elastomer and curing agent were purchased from Sylgard®. PTFE syringe filters (0.45 µm) were purchased from Lab Unlimited (Dublin). Full-fat milk and Aptamil® Follow on Milk infant formula were purchased from a local supermarket. 4-aminothiophenol (4-ABT), 1-decanethiol (DT) and mercaptohexanol (MH) were prepared by dissolving in ethanol. All standards of crystal violet (CV), melamine, and glucose were prepared as required, using deionized water (18.2 MΩ.cm ELGA Pure Lab Ultra systems) and a serial dilution method employed to prepare standards in the desired concentration ranges. HPLC primary stock solutions of melamine were prepared in deionized water at a concentration of 10 ppm. Working standards were prepared in the range 0.1 ppm – 5.0 ppm using deionized water. For electrospray ionization mass spectrometry (ESI-MS) measurements, milk samples were diluted with deionized water (1:10) and passed through a 0.45 µm syringe filter to prevent blockage during infusion. Both melamine-spiked and unspiked milk samples were prepared in the same manner. All standard solutions were stored at room temperature 18 ºC.

2.2. Fabrication of SERS Substrate

To prepare the Al templates, the outer (printed side) of an Al soda can was sanded using fine (P120, ~125 µm particle size) and extra fine (P280, ~50 µm) grade sandpaper to remove the paint then cut into 1 cm^2 pieces. ~~This was then followed by a polish using~~ The can pieces were then polished with 6 µm and 1 µm alumina slurry, until they appeared shiny, to smoothen the deformities caused by sanding the Al surface. Finally, the Al template preparation was finished with a chemical bath (5% NaOH, 2-3 minutes) which dissolved the top Al surface. This reduced inhomogeneous surface asperities and removed sanding debris. Pellets of PVDF and PS were placed on separate microscope slides and melted on a hotplate. The prepared Al masters, see Fig. S1, were then placed onto the melted droplets and pushed downward so the respective polymers wetted the Al. The glass slides were removed from the hotplate and allowed cool whereon the polymers could be easily peeled from both the glass slides and Al templates, Fig 1(b), to yield a flexible transparent polymer bases, Fig 1(c). Concerning PDMS silicone elastomer, Sylgard 184 base and the curing agent were mixed in a 10:1 ratio and degassed under partial vacuum to remove bubbles. In a petri dish, the PDMS pre-polymer was poured over the Al master and heat cured at 60°C for 1 hour. The Al pieces were again peeled from the flexible polymer to yield nanostructured PDMS surfaces. To complete substrate fabrication, a thin Ag layer (30 nm) was then deposited onto the different polymer bases by thermal evaporation (Edwards Autocore 500, 3×10^{-7} bar, ~1.6 A). The thickness and the deposition rate were controlled in situ using a calibrated quartz microbalance. Control substrates were also fabricated as above where the Al master template was replaced with glass slides, yielding a smooth unpatterned surface.

2.3. Characterisation of SERS substrates

Scanning electron microscopy analysis was undertaken to characterize the substrate surface after the fabrication procedure. SEM images were acquired using a calibrated field emission SEM (JSM-7500F, JEOL UK Ltd.) operating at beam voltages between 3 and 5 kV. All Raman measurements were recorded using a Confocal Renishaw Raman Microscope equipped with a 514 nm Ar ion laser and analysed using Wire 3.0 computer software. The laser spot diameter was ~1 µm at the substrate surface and a laser power density of $\sim7\times10^4$ W/cm^2 was used. SERS spectra were obtained by averaging 5 random accumulations, collected using a 50x magnification (0.75 NA) objective microscope, with a data acquisition time of 10 s, over an extended spectral range of 200 cm^{-1} to 3500 cm^{-1}. The spectrometer was equipped with a computer controlled motorised XYZ stage employed to focus and adjust the positioning of the sample on the silver surface. Subtraction of the baseline was performed on all spectra to eliminate background noise from the underlying polymer and the recorded spectra were imported into Origin® 7.4 (OriginLab) to facilitate data analysis.

2.4. FEM Simulations

The electromagnetic response of the nanostructure was simulated by the finite element method (FEM) with a commercial software package (COMSOL Multiphysics with Wave Optics and CAD Import Modules). To construct a 3D image of the sample, the pixel value (pv) of the greyscale, 16 bit SEM micrograph was converted into height (h) with the following algorithm: if pv < 15000, h = 0 and if 15000 ≤ pv ≤ 65000, h = 30*(pv - 15000) /(50000). With this conversion, black areas with pixel values below 15000 corresponded to 0 nm and white areas with a pixel value of 65000 to 30 nm. This converted image was used as a parametric surface in COMSOL. The 3D geometry was then constructed by intersecting the parametric surface with blocks. This resulted in three domains, i.e. the Ag nanocluster with a PVDF substrate and an air superstrate. These domains were meshed with tetrahedral elements with a minimum size of 0.03 nm. A total volume of 100 x 100 x 150

nm^3 was chosen to keep the computational demand manageable for a 3.50 GHz, quad core, 16 GB RAM PC. The refractive index of air, PVDF and Ag were 1; 1.42 and 0.14 +2.91, respectively.[50] A 5 nm perfectly matched layer was considered on all sides of the structures, as well as above the air superstrate and below the PVDF substrate. A 514 nm plane wave Einc with a power of 1 W (corresponding to an electromagnetic field magnitude of 3×10^7 V/m) and a polarization along the Y axis was inputted and COMSOL solved for full field Etot. The enhancement factor G can be calculated as G= (Etot /Einc).

2.5. SERS Chemical analysis

To explore the suitability of these substrates for highly sensitive measurements, a series of crystal violet standards ranging from 10^{-7} to 10^{-10} M were prepared in DI water and deposited via the drop/dry process on the substrates; depositing 50 µl of solution onto the substrate and allowing to air dry (10 minutes). All samples were thoroughly rinsed with DI water before Raman analysis to remove unadsorbed, clumped molecules that accumulated on the surface of the substrate during the drying process. 50 µL aliquots (10^{-6} M) of malachite green (in DI water), imidacloprid (in methanol and DI water), benzocaine (in DI water) and 4-ABT (in 97% ethanol) were also deposited and analysed in a similar manner.

Glucose: Glucose detection was undertaken using a similar method to Van Duyne et al.[47] DT/MH (1-decanethiol, mercaptohexanol) functionalisation of the Ag surface was first undertaken to yield a mixed thiol self-assembled monolayer (SAM). Substrates were incubated in 1 mM DT for 45 minutes followed by incubation in 1 mM MH for 24 hours. A Raman analysis was undertaken at this point to obtain the SAM spectra. The substrate is then immersed into 10 mM of aqueous glucose solution for 6 hours, air dried and Raman analysis was undertaken.

Melamine: Working solutions of infant formula were first prepared using manufacturer instructions, then by diluting 1:10 with D.I. water. Working solutions of full-fat milk were similarly prepared using a 1:10 dilution step. Melamine was dissolved by sonication using the appropriate working solutions to yield 10 ppm (w/v) stock solutions. A further 1:10 dilution was then undertaken to prepare 1 ppm standard solutions. No further sample preparation was undertaken. A drop/dry method was again employed for these experiments; depositing 50 µl of solution onto a substrate and allowing to air dry (10 minutes).

2.6. Melamine Direct Infusion EIS-MS Analysis

As prepared melamine and full-fat milk 10 ppm stock solutions were diluted with appropriate volumes of working solutions to yield 0.5, 1, 1.5, 2, 3, 4, & 5 ppm solutions. Both melamine-spiked and unspiked milk samples were diluted with deionized water (1:10 dilution) and passed through a 0.45 µm syringe filter to prevent blockage during ESI infusion. Individual 500 µL glass syringes (Hamilton – Bonaduz, Schweiz (Gastight ® # 1750)) were then filled with these melamine standards followed by infusion into the ESI source of an Agilent 6340 series ion trap mass spectrometer (flow rate of 10 µL min^{-1}). The instrument was calibrated following the manufacturer guidelines and using Agilent ESI Tuning Mix (G2431A 100 ml acetonitrile solution for Ion-trap MS). For MS, a positive ESI mode with nebulizer pressure at 15 psi was employed. Nitrogen was used as the drying gas under a flow of 5 L min^{-1} and a temperature of 325 °C. Acquisition and analysis of data were performed with Agilent ChemStation LC and 6300 Series Trap Control (version 6.2). Library building and spectral matching were conducted using DataAnalysis™ and LibraryEditor™ software (Bruker Daltonik GmbH). ESI-MS conditions were initially optimized by directly infusing melamine standard (0.1 – 200 ppm) and varying the amplitude for both MS^2 and MS^3. The optimized conditions for the MS^2 fragmentation of precursor ion [m/z 127] was determined to have an amplitude of 0.5 and the optimized conditions for MS^3 fragmentation was determined to be an amplitude of 0.4.

3. Results and Discussion

3.1. Substrate Fabrication

Briefly, a polished soda can (cf. methods section) was used to template a pre-polymer generating a nanostructured surface, illustrated schematically in Fig. 1 (a). After the templating process, the polymer was released from the glass support and the Al template easily peeled away to yield a flexible transparent polymer base, Fig. 1 (b-c). Ag was then thermally deposited (30 nm) onto nanopatterned polymer substrates to complete substrate fabrication, Fig. 1 (d). SEM analysis was undertaken following substrate preparation. ~~PVDF substrates that were fabricated with Al templates that had only been sanded, i.e. no polishing, displayed micron-sized defects and scratches across the substrate surface. However, the addition of polishing steps (alumina slurry followed by a NaOH wash) greatly eliminated these defects and the substrates exhibited a nanostructured and relatively defect-free surface.~~ Fabrication included removing the Al can's print using rough sandpaper. As expected, this process yielded micron-sized scratches across the Al surface. Subsequently, Raman enhancement was negligible from these substrates, as a result of the large surface roughness. The introduction of polishing steps (alumina slurry followed by a NaOH wash) smoothened the surface and greatly reduced the sanding scratches, producing polymer substrates that yielded a considerable SERS effect. Fig. 1 (d) shows a typical SEM micrograph of a portion of a fully prepared PVDF substrate following Ag deposition. From SEM analysis the size distribution of the Ag nano-structures was estimated to be roughly 60 ± 20 nm while the gaps between the clusters were estimated to be on the order of 10 ± 5 nm (inset Fig. 1 (d)) with the Ag nanostructures uniformly distributed over the entire PVDF surface. These well-defined structures, comprising such small separations between clusters, are expected to deliver a high yield of hot-spots, making them very attractive and suitable for SERS sensing. Visual inspection of the fabricated SERS substrates displayed a uniform non-reflective finish, suggesting a roughened surface. By contrast, un-templated "smooth" control substrates displayed a mirror finish following Ag deposition.

3.2. ~~Structural Characterisation~~ Substrate Characterisation

Three different polymers PVDF, PS and PDMS were assessed for fabrication of the SERS substrate. PDMS was selected since it is a well-characterised material that is well known to replicate and template nanostructure surfaces.[51, 52] Similarly, PS has also been employed to template nanostructures[27] as it is known to form ~~forming~~ rigid homogenous surfaces, while PVDF was selected as it is a known piezoelectric polymer.[53] SERS analysis was first undertaken on bare Ag substrates, Fig S2, i.e. no molecule deposition. This allows the examination the Raman active modes of the three selected polymers. As expected, all three polymers produced the same roughened Ag surface from the Al master, however the SERS responses were not equivalent. It was observed that the more SERS active the polymer was, the more it interfered with the SERS response of the deposited molecule. Then we employed both CV and 4-ABT to compare and evaluate the SERS properties of each polymer substrate, see Fig S3. These experiments demonstrated that PVDF produced the optimal SERS surface, providing the largest SERS enhancement for both molecules and the least background interference. We established that PDMS produced a high signal enhancement, similar to PVDF, but had poor adhesion to the deposited Ag (failed tape test). PS was rigid but fragile (shattered easily under stress) and produced a considerably weaker SERS response. ~~We also explored direct deposition of Ag onto polished Al substrates directly. The results (see Fig. S2) show that the Al substrate appeared to quench the SERS enhancement of CV, resulting in a reduced SERS response.~~ We also explored using the Al master as the substrate, by depositing Ag directly onto the polished Al surface. Fig. S4 shows a comparison between a PVDF substrate and the Al substrate. There is a slight response from the nanostructured metal, however the spectrum has considerable changes when

compared to the polymer substrate. Weak signals are observed for the strongest vibrations modes at 1620, 1386 and 915 cm^{-1} from the Al sample and a number of characteristic CV peaks are not detected. The non-plasmonic Al metal appears to quench the SERS enhancement of CV provided by electromagnetic effect, resulting in a reduced SERS response.

Different Ag film thicknesses (10, 30 and 50 nm) on PVDF substrates were also explored. SEM analysis of the 10 nm Ag substrates showed large separations between Ag clusters while the spectra obtained from different locations varied significantly and produced very little SERS enhancement (see Fig. S5 (a-b)). SEM analysis of the 50 nm Ag substrates showed an almost continuous film with small numbers of separations visible and corresponding spectra exhibiting lower SERS enhancement compared to the 30 nm thick films, due to the lack of hot spots (see Fig. S5 (c-d)). Finally, 30 nm thick Ag films exhibited excellent SERS response, and were thus selected for use in this work and will be discussed in detail below.

3.3. Simulations

Concerning the 30 nm thick Ag deposited films, Fig. 2 (a) shows a typical SEM image of a portion of a substrate. The dimensions of the Ag clusters were roughly 60 ± 20 nm while the separations between the clusters were estimated to be 10 ± 5 nm. Finite element method simulations were undertaken to explore if these metal-dielectric-metal nanogap structures were sufficient to produce localised significant electric field enhancements and consequently act as hotspots when illuminated with incident light (514 nm). A portion of a SEM image highlighted by the dashed box in Fig. 2 (a) was imported and rendered in Comsol Multiphysics™ see Fig. 2 (b). Fig. 2 (c) shows the total electric field map 2 nm above the surface when the sample is illuminated with a light polarized along the y-axis. As can be seen, a very high electric field ($E \sim 10^8$ V/m) is concentrated on the edges of the Ag nanoclusters that are perpendicular to the axis of polarization of the incident light. A cross section of the substrate, Fig. S6, shows that the field enhancement is not confined to the surface of the nanoclusters but rather extends to the whole gap. This is characteristic of coupling of the individual localised surface plasmon modes of the adjacent nanoclusters. These simulations confirm that the substrates fabricated using the templates technique should be sufficient to create nanogaps that will, on illumination, create electromagnetic hot spots and that most of the SERS signal recorded from the sample will originate from molecules located in these nanogaps.

3.4. SERS Characterisation

To validate the simulation model and confirm that the origin of the observed SERS responses arose from the metal-dielectric-metal nanogap structures, a number of control experiments were undertaken: (i) smooth substrates were prepared by depositing 30 nm of Ag onto smooth PVDF films, i.e., no templated nanostructures and (ii) Ag-coated nanostructured PVDF samples in the absence of CV. Spectra obtained following front "top excitation" are shown in Fig. 3 (a). No appreciable Raman signals were observed from the control experiments (black and green spectra, respectively). By contrast, spectra recorded using Ag coated nanostructured PVDF substrates in the presence of CV (blue spectrum) show a significant SERS response. Such results strongly support the simulation model suggesting that the nanogap structures between nanostructured Ag clusters created hotspots for efficient SERS enhancement to occur. The exhibited spectral peaks at 914, 1176, 1376 and 1618 cm^{-1} for CV were assigned (see, Table S1) and compared to those exhibited in bulk Raman spectra (see, Fig. S7) and were in accordance with previously reported values [12, 54].

The intensity of the SERS enhancements of particular Raman modes depends on the formation of, and interaction between, the Ag surface and the adsorbed molecule. To calculate the enhancement factor (EF), CV vibrations at 1620, 1175 and 914

cm^{-1} from Fig. 3 (a) and Fig. S7 (bulk CV Raman spectrum) were analysed. A detailed description of EF calculations is provided in the supporting information section. Briefly, EF values were calculated using the equation: [55]

$$EF = \frac{I_{SERS} / N_{SURF}}{I_{NR} / N_{VOL}}$$

Where *I* is the intensity of a band in the SERS spectrum (I_{SERS}) and the normal Raman spectrum (I_{NR}), and *N* is the average number of molecules, in the scattering volume, adsorbed on SERS substrate (N_{SURF}) and in the CV powder (N_{VOL}). For the vibrational peak at ~1620 cm^2 the intensities for SERS and Raman are 126,215 and 2,008 a.u. respectively, and the enhancement factor was calculated as 2.41×10^6. The vibrational bands at 1175 cm^{-1} and 913 cm^{-1} exhibited EFs of 1.62×10^6 and 1.36×10^6 respectively. Such enhancements compare well with those reported in the literature [43, 56, 57]. However, CV exhibits a maximum absorption peak at 590 nm.[58] Theoretically, the 514 nm laser used in these experiments could increase the observed SERS enhancements, due to resonance effects at this wavelength, i.e., a chemical effect. To explore if this is the case, analysis was undertaken on the non-resonant molecule, 4-ABT, and the enhancement factor calculated was consistent to that shown here (cf: Supp info). It was found that the EF values for the non-resonant 4-ABT molecule were similar to those of resonant CV. Thus we consider the SERS enhancements observed with these substrates arise predominantly from an electromagnetic effect.

3.5. Back excitation

A key advantage of the Ag coated PVDF substrates is that they are optically transparent in the visible spectrum which enables back excitation (though substrate) SERS measurements to be undertaken. Such a capability is important for many industrial in-line process analytical monitoring techniques (PAT) used in smart manufacturing 4.0 approaches. Back excitation SERS measurements, i.e. illumination and collection through the back facet of the substrate were undertaken; see Fig. 3 (b). A typical SERS spectrum using back excitation from 10^{-6} M CV (red spectrum) is shown and exhibited characteristic spectral peaks at 914, 1176, 1376 and 1618 cm^{-1} as described previously. In the absence of CV (green spectrum), there is a weak signal contribution from the PVDF, but it does not cause any significant SERS interferences, as expected from the front excitation experiments in Fig. S3. Fig. 3 (c) shows a direct comparison between the front and back excitation intensities for the peak at 1620 cm^{-1}. Although there is a threefold decrease in the measured intensity (compared with front excitation), since these spectra were acquired through a thick PVDF base, (3 mm) we believe that if thinner substrates were employed (by optimizing the fabrication process further), reduced light scattering within the substrates would result in a larger measured SERS enhancements.

To explore back excitation further, a 50 µL droplet of CV (10^{-6} M) was deposited onto a substrate and overlaid with a glass coverslip to form a fluid-type cell with a thickness of ~ 100 µm, see inset image of Fig. 4 (b). If the molecule was simply dropped on the surface and allowed dry, due to the surface hydrophobicity, there would be very little wetting and we would observe localised pre-concentration of the target analyte on the Ag surface [27, 59]. In this case, we spread the droplet across the Ag surface using the cover slip, i.e. undertaking the SERS measurements through the back of the polymer with liquid on the metal surface. We believe that as the liquid dries, the CV molecules can pre-concentrate in the remaining liquid also that slower the drying process allows the CV molecules to adsorb more evenly across the entire surface. A number of SERS spectra were acquired (in the same position) through the polymer substrate over a 45-minute time frame. Fig. 4 (a) shows a waterfall plot of CV spectra. During these experiments, a SERS response was observed after 1 minute and, as expected,

higher SERS signal intensities were observed with increasing time and eventually saturated. Fig. 4 (b) illustrates a plot of peak area (913 cm^{-1} calculated using a Lorentzian function) vs. time; yielding a linear relation (R^2 of 0.98). We suggest that the increase in signal arises from the ~~pre-concentration~~ adsorption of the CV molecules to the metal surface, as the droplet dries. ~~These results strongly~~ The ability of these substrates to undertake SERS in liquid samples supports the suggestion that these transparent polymer substrates could find use in future in-line measurement applications required in process analytical technologies. This ability to undertake back excitation SERS could also open up other new remote sensing application areas if, for example, the substrates are integrated with optical emitters or at the end of optical fibers such enabling, e.g., in-vivo measurements or used for in-line measurement.

3.6. Quantitative analysis

Concerning quantitative analysis, a series of CV standards ranging from 10^{-7} to 10^{-10} M were prepared. (*cf:* material and methods). SERS spectra were obtained by measuring and averaging five different locations on a substrate for each concentration. The averages of five spectra for each concentration are presented in Fig. 5 (a). As illustrated, all the characteristic CV peaks are well defined (even at such low concentrations 5 x 10^{-10}). The vibration peak at 915 cm^{-1} was selected for calibration measurements and the peak area (averaged for each standard) was determined using a Lorentz function in Origin® 7.4 (OriginLab) and plotted versus log of concentration to obtain a quantitative calibration curve, see Fig. 5 (b). Regression analysis was then undertaken and a correlation coefficient (R^2) of 0.9794 was obtained with a measured limit of detection of 5 x 10^{-10} M. The results show that the SERS substrates permit rapid analysis times (~10 min from sample deposition). To evaluate the reproducibility and homogeneity of the substrates, Fig. 5 (c) shows a waterfall graph for at 48 spectra (10^{-6} M CV concentration) taken from 4 random locations in grids of 10 μm^2 (12 spectrum per grid) on a single substrate (north, south, east and west separated by 5 mm). The relative standard deviation for each of the peaks; 1620, 1587, 1174 and 913 cm^{-1}, were calculated as less than 15%.

3.7. Versatility & stability

To evaluate the versatility of the SERS substrate, various chemicals were analysed from different application fields; imidacloprid (neonicotinoid pesticide), melamine (previously used as a food adulterant), malachite green (agricultural antibiotic) and benzocaine (pharmaceutical molecule), see Fig. 5 (d). The characteristic SERS peaks of all four molecules, in aqueous solution at a concentration of 10^{-6} M, are clearly resolved and correlate well to those reported in the literature. [38, 60-63] The stability of the PVDF polymer substrates was also assessed. Substrates were found to be stable following immersion in a wide range of acids (acetic, nitric, hydrochloric sulfuric and phosphoric acids) as well as most bases. They also upheld their integrity after prolonged exposure to both polar and non-polar solvents (methanol, ethanol, DMSO, toluene and hexane) for up to 20 minutes. However, a notable exception was that PVDF had low resistances to sodium hydroxide and acetone. Exposure to these solutions caused breakdown of the polymer base and deformation of the Ag surface. It was found that a single Al substrate may also be re-used to template multiple PVDF SERS substrates. Fig. S8 (a) shows spectra obtained from substrates templated with both a pristine and re-used Al master. ~~although there is a slight decrease in the intensity of the spectrum obtained from the second replicate sample,~~ The close reproducibility of the data indicated that the templating procedure does not damage the aluminum template. Polymer SERS substrates were also cleaned using a combination of a sonicated solvent wash (5 mins in isopropanol/ 5 mins in ethanol) followed by exposure to UV-ozone (20

min at ambient pressure) and re-used for analysis of 10^{-6} M CV (at least four times) without any signal degradation, see Fig. S8 (b).

The SERS substrates may also be applied to molecules, such as glucose, that have a poor binding affinity for the substrates Ag surface. In a manner similar to that reported by the Van Duyne group [47], a mixed self-assembled monolayer of mercaptohexanol and decanethiol was first employed to partition glucose from solution at a SERS sensor surface. The two thiols, having different length hydrocarbon chains, created "pockets" in the monolayer, shown schematically in Fig. 6 (a), which promoted glucose partitioning to this modified surface via the formation of both Van Der Vaal and hydrogen bonding interactions. Fig. 6 (b) shows a typical spectrum obtained for the as-deposited SAM layer (control sample, black spectrum) exhibiting a weak SERS response with peaks at 1122, 891 and 710 cm^{-1}. Following immersion in a 10 mMol glucose solution for 6 hours and air drying, a spectrum for the combined SAM / sequestered glucose layer was observed (dotted line spectrum). This spectrum contains vibrational peaks from both the SAM layer and glucose analyte. Finally, the glucose spectrum, obtained by subtracting the SAM spectrum from the combined glucose/SAM spectrum, is presented (blue spectrum). The resulting spectrum exhibited characteristic glucose peaks at 1434 1123, 1065, 912, 893, 710 and 542 cm^{-1}, which compare with both the literature and a characteristic Raman spectrum obtained from bulk glucose (see Fig. S9) [64].

Finally, a case study was undertaken to demonstrate the suitability of these substrates for real world applications, e.g in food security. Melamine, a food adulterant, previously used to falsify protein content in milk products in China[65, 66] and which is known to be difficult to detect was selected for this study. [49] A typical SERS spectrum for 1 ppm melamine in deionized water is presented in Fig. 7 (a). The characteristic peak observed at ~702 cm^{-1} is attributed to the breathing mode and in plane deformation of the triazine ring[67, 68] while the 855 cm^{-1} peak is attributed to the out of plane ring deformation.[69] These peaks correspond well with reported values.[68] Fig. 7 (b) shows spectra obtained from 1 ppm melamine-spiked into both milk and baby formula (diluted 1/100 as described in the experimental section). Control samples of diluted milk and baby formula were also analysed and the absence of SERS responses from these solutions showed that other large biomolecules (fats, proteins etc.) present in these solutions would not interfere with the melamine analysis By contrast, the melamine-spiked milk and baby formula samples exhibited characteristic melamine peaks, clearly distinguishable from the pristine solution spectra, confirming the presence of melamine even at very low concentrations, i.e., 1 ppm. A drop and dry approach was again adopted, the total analysis time was under 10 minutes and a LOD of 0.1 ppm was measured experimentally. These results suggest that these substrates may offer the possibility for the rapid detection of analytes in the field, with a limit of detection similar to gold standard laboratory-based techniques such as mass spectrometry.

To this end, the SERS detection method was benchmarked against electrospray ionization mass spectrometry (ESI-MS). The spiked melamine solutions were analysed with the MS, operated in single reaction monitoring positive mode, and the ion charge control function used to optimize both MS^2 and MS^3 fragmentation. Total ion count, MS^2 and MS^3 data were obtained. Fig. 8 (a) shows MS^2 and MS^3 mass spectra obtained for the direct infusion of melamine standard (0.1 ppm) spiked into deionised water. Fig. 8 (b) shows MS^2 and MS^3 mass spectra obtained for the direct infusion of melamine standard (10 ppm) spiked in a diluted (1 in 10, DI) milk sample. MS^2 fragmentation of precursor ion at *m/z* 127 yielded five predominant characteristic product ions at *m/z* 109, 97, 84, 85 and 69 while MS^3 fragmentation of product ions at *m/z* 109 yielded the predominant product at *m/z* 81. The spectra obtained for MS^2 and MS^3 for melamine correlated with spectra obtained in

previously published studies[70]. In agreement with the SERS study, no trace of melamine was found in control pristine milk samples.

The SERS substrates exhibited a similar sensitivity to the ESI-MS data for melamine in water (LOD, 0.1 ppm) and for melamine detection in diluted milk samples (1 ppm). These results are very encouraging and demonstrate that our fabricated SERS substrates exhibit sensitivities comparable to the gold standard analytical technique. However, the ESI-MS samples did require the use of a syringe filter to remove any large interferences in the milk including proteins and lipids that masked the melamine signal. SERS, on the other hand, had the ability to selectively detect melamine in spiked milk samples without sample pretreatment (due to the lack of a background signal). These results strongly support the assertation that SERS substrates offer the possibility for rapid and low-cost detection of target analytes in complex media, in remote settings.

Conclusion

In conclusion, we demonstrated the reproducible fabrication of a polymer based SERS substrate; nanostructured using a soda can as a template. The Ag coated PVDF exhibited strong SERS enhancement with good metal adhesion compared to PDMS and PS polymers. Simulations and control experiments confirmed that the Raman signal arose from the gaps ("hot spots") between the Ag clusters throughout the Ag layer. The substrates exhibited an enhancement factor of ~10^6 and that the signals observed with these substrates arose predominantly from an electromagnetic effect. The transparent substrates also permitted back excitation and collection through the substrate which corresponding spectra exhibiting clear and defined spectral SERS peaks. The versatility of the sensors was demonstrated by detection of a wide variety of analytes on pristine Ag surfaces. The sensors exhibited rapid, quantitative and high sensitivity, for example, 5 x 10^{-10} M (204 pg/mL) crystal violet detection in 10 minutes using a simple drop and dry method. We also show detection of glucose employing a chemically modified Ag surface bearing a pre-deposited SAM layer. Finally, we present the detection of trace amounts of melamine in complex media solution (milk and infant formula) and show the sensor sensitivity is comparable with commercial analytical instrumentation (MS-MS). On-going work is now focusing on exploring these sensor substrates to detect, identify and measure trace amounts of pesticides in aqueous solutions for use in food safety, applications.

Acknowledgement

This work was supported in part by Science Foundation Ireland under the US-Ireland Program (SFI12/US/I2476), supported in part by a research grant from Science Foundation Ireland (SFI) under the European Regional Development Fund under Grant Number 13/RC/2077 and by the European Commission under the FP7 Project Phast-ID (258238).

References

[1] J. Kong, M.G. Chapline, H. Dai, Functionalized carbon nanotubes for molecular hydrogen sensors, Advanced Materials, 13(2001) 1384.

[2] G. Zheng, F. Patolsky, Y. Cui, W.U. Wang, C.M. Lieber, Multiplexed electrical detection of cancer markers with nanowire sensor arrays, Nat Biotech, 23(2005) 1294-301.

[3] M.-Y. Tsai, N. Creedon, E. Brightbill, S. Pavlidis, B. Brown, D.W. Gray, et al., Direct correlation between potentiometric and impedance biosensing of antibody-antigen interactions using an integrated system, Applied Physics Letters, 111(2017) 073701.

[4] A.P. Alivisatos, W. Gu, C. Larabell, Quantum dots as cellular probes, Annu Rev Biomed Eng, 7(2005) 55-76.

[5] J.M. McMahon, J. Henzie, T.W. Odom, G.C. Schatz, S.K. Gray, Tailoring the sensing capabilities of nanohole arrays in gold films with Rayleigh anomaly-surface plasmon polaritons, Optics express, 15(2007) 18119-29.

[6] P. Lovera, D. Jones, B. Corbett, A. O'Riordan, Polarization tunable transmission through plasmonic arrays of elliptical nanopores, Optics express, 20(2012) 25325-32.

[7] M.G. Albrecht, J.A. Creighton, Anomalously intense Raman spectra of pyridine at a silver electrode, Journal of the American Chemical Society, 99(1977) 5215-7.

[8] D.L. Jeanmaire, R.P. Van Duyne, Surface raman spectroelectrochemistry: Part I. Heterocyclic, aromatic, and aliphatic amines adsorbed on the anodized silver electrode, Journal of Electroanalytical Chemistry and Interfacial Electrochemistry, 84(1977) 1-20.

[9] R. Botta, G. Upender, R. Sathyavathi, D. Narayana Rao, C. Bansal, Silver nanoclusters films for single molecule detection using Surface Enhanced Raman Scattering (SERS), Materials Chemistry and Physics, 137(2013) 699-703.

[10] S. Nie, S.R. Emory, Probing single molecules and single nanoparticles by surface-enhanced Raman scattering, Science, 275(1997) 1102-6.

[11] A. Otto, Theory of first layer and single molecule surface enhanced Raman scattering (SERS), Phys Status Solidi A, 188(2001) 1455-70.

[12] K. Kneipp, Y. Wang, H. Kneipp, L.T. Perelman, I. Itzkan, R. Dasari, et al., Single molecule detection using surface-enhanced Raman scattering (SERS), Physical Review Letters, 78(1997) 1667-70.

[13] J.R. Lombardi, R.L. Birke, G. Haran, Single Molecule SERS Spectral Blinking and Vibronic Coupling, The Journal of Physical Chemistry C, 115(2011) 4540-5.

[14] D.-K. Lim, K.-S. Jeon, H.M. Kim, J.-M. Nam, Y.D. Suh, Nanogap-engineerable Raman-active nanodumbbells for single-molecule detection, Nat Mater, 9(2010) 60-7.

[15] L. Yang, L. Ma, G. Chen, J. Liu, Z.-Q. Tian, Ultrasensitive SERS Detection of TNT by Imprinting Molecular Recognition Using a New Type of Stable Substrate, Chemistry – A European Journal, 16(2010) 12683-93.

[16] W. Xie, S. Schlucker, Medical applications of surface-enhanced Raman scattering, Physical Chemistry Chemical Physics, 15(2013) 5329-44.

[17] M. Fleischmann, P.J. Hendra, A.J. McQuillan, Raman spectra of pyridine adsorbed at a silver electrode, Chem Phys Lett, 26(1974) 163-6.

[18] M. Moskovits, Surface-enhanced spectroscopy, Reviews of Modern Physics, 57(1985) 783-826.

[19] A. Otto, I. Mrozek, H. Grabhorn, W. Akemann, Surface-enhanced Raman scattering, Journal of Physics: Condensed Matter, 4(1992) 1143.

[20] P.L. Stiles, J.A. Dieringer, N.C. Shah, R.P.V. Duyne, Surface-Enhanced Raman Spectroscopy, Annual Review of Analytical Chemistry, 1(2008) 601-26.

[21] M. Kahl, E. Voges, S. Kostrewa, C. Viets, W. Hill, Periodically structured metallic substrates for SERS, Sensors and Actuators B: Chemical, 51(1998) 285-91.

[22] Q. Yu, P. Guan, D. Qin, G. Golden, P.M. Wallace, Inverted Size-Dependence of Surface-Enhanced Raman Scattering on Gold Nanohole and Nanodisk Arrays, Nano Letters, 8(2008) 1923-8.

[23] S. Krishnamoorthy, S. Krishnan, P. Thoniyot, H.Y. Low, Inherently Reproducible Fabrication of Plasmonic Nanoparticle Arrays for SERS by Combining Nanoimprint and Copolymer Lithography, ACS Applied Materials & Interfaces, 3(2011) 1033-40.

[24] E.D. Diebold, N.H. Mack, S.K. Doorn, E. Mazur, Femtosecond Laser-Nanostructured Substrates for Surface-Enhanced Raman Scattering, Langmuir, 25(2009) 1790-4.

[25] J.C. Hulteen, D.A. Treichel, M.T. Smith, M.L. Duval, T.R. Jensen, R.P. Van Duyne, Nanosphere Lithography: Size-Tunable Silver Nanoparticle and Surface Cluster Arrays, The Journal of Physical Chemistry B, 103(1999) 3854-63.

[26] M. Fan, G.F.S. Andrade, A.G. Brolo, A review on the fabrication of substrates for surface enhanced Raman spectroscopy and their applications in analytical chemistry, Anal Chim Acta, 693(2011) 7-25.

[27] P. Lovera, N. Creedon, H. Alatawi, M. Mitchell, M. Burke, A.J. Quinn, et al., Low-cost silver capped polystyrene nanotube arrays as super-hydrophobic substrates for SERS applications, Nanotechnology, 25(2014) 175502.

[28] S.J. Lee, A.R. Morrill, M. Moskovits, Hot Spots in Silver Nanowire Bundles for Surface-Enhanced Raman Spectroscopy, Journal of the American Chemical Society, 128(2006) 2200-1.

[29] M.J. Banholzer, J.E. Millstone, L. Qin, C.A. Mirkin, Rationally designed nanostructures for surface-enhanced Raman spectroscopy, Chemical Society Reviews, 37(2008) 885-97.

[30] S.E. Bell, M.R. McCourt, SERS enhancement by aggregated Au colloids: effect of particle size, Physical Chemistry Chemical Physics, 11(2009) 7455-62.

[31] M. Grzelczak, J. Vermant, E.M. Furst, L.M. Liz-Marzán, Directed Self-Assembly of Nanoparticles, Acs Nano, 4(2010) 3591-605.

[32] S. Zhu, C. Fan, J. Wang, J. He, E. Liang, Self-assembled Ag nanoparticles for surface enhanced Raman scattering, Optical Review, 20(2013) 361-6.

[33] L. Zhang, Self-assembly Ag nanoparticle monolayer film as SERS Substrate for pesticide detection, Applied Surface Science, 270(2013) 292-4.

[34] M. Hepel, C.-J. Zhong, Functional Nanoparticles for Bioanalysis, Nanomedicine, and Bioelectronic Devices Volume 2, ACS Symposium Series, American Chemical Society2012, p. 0.

[35] J. Tang, Q. Zhao, N. Zhang, S.-Q. Man, Facile fabrication of large-area and uniform silica nanospheres monolayer for efficient surface-enhanced Raman scattering, Applied Surface Science, 308(2014) 247-52.

[36] W. Li, P.H.C. Camargo, X. Lu, Y. Xia, Dimers of Silver Nanospheres: Facile Synthesis and Their Use as Hot Spots for Surface-Enhanced Raman Scattering, Nano Letters, 9(2009) 485-90.

[37] A. Martín, A. Pescaglini, C. Schopf, V. Scardaci, R. Coull, L. Byrne, et al., Surface-Enhanced Raman Scattering of 4-Aminobenzenethiol on Au Nanorod Ordered Arrays, The Journal of Physical Chemistry C, 118(2014) 13260-7.

[38] A. Martin, J.J. Wang, D. Iacopino, Flexible SERS active substrates from ordered vertical Au nanorod arrays, RSC Advances, 4(2014) 20038-43.

[39] Z. Xie, J. Tao, Y. Lu, K. Lin, J. Yan, P. Wang, et al., Polymer optical fiber SERS sensor with gold nanorods, Opt Commun, 282(2009) 439-42.

[40] D.A. Walker, K.P. Browne, B. Kowalczyk, B.A. Grzybowski, Self-Assembly of Nanotriangle Superlattices Facilitated by Repulsive Electrostatic Interactions, Angewandte Chemie International Edition, 49(2010) 6760-3.

[41] Z. Liu, Z. Yang, B. Peng, C. Cao, C. Zhang, H. You, et al., Highly Sensitive, Uniform, and Reproducible Surface-Enhanced Raman Spectroscopy from Hollow Au-Ag Alloy Nanourchins, Advanced Materials, 26(2014) 2431-9.

[42] M. Yang, R.n. Alvarez-Puebla, H.-S. Kim, P. Aldeanueva-Potel, L.M. Liz-Marzán, N.A. Kotov, SERS-Active Gold Lace Nanoshells with Built-in Hotspots, Nano Letters, 10(2010) 4013-9.

[43] A. Kudelski, Raman studies of rhodamine 6G and crystal violet sub-monolayers on electrochemically roughened silver substrates: Do dye molecules adsorb preferentially on highly SERS-active sites?, Chem Phys Lett, 414(2005) 271-5.

[44] S. Srivastava, R. Sinha, D. Roy, Toxicological effects of malachite green, Aquat Toxicol, 66(2004) 319-29.

[45] N.A. Littlefield, B.-n. Blackwell, C.C. Hewitt, D.W. Gaylor, Chronic Toxicity and Carcinogenicity Studies of Gentian Violet in Mice, Toxicological Sciences, 5(1985) 902-12.

[46] E. Commission, Minimum Required Performance Limit (MRPL) for malachite green, in: E. Commission (Ed.)2002.

[47] O. Lyandres, N.C. Shah, C.R. Yonzon, J.T. Walsh, M.R. Glucksberg, R.P. Van Duyne, Real-Time Glucose Sensing by Surface-Enhanced Raman Spectroscopy in Bovine Plasma Facilitated by a Mixed Decanethiol/Mercaptohexanol Partition Layer, Analytical Chemistry, 77(2005) 6134-9.

[48] Z. Chen, X. Yan, Simultaneous Determination of Melamine and 5-Hydroxymethylfurfural in Milk by Capillary Electrophoresis with Diode Array Detection, J Agr Food Chem, 57(2009) 8742-7.

[49] Y. Liu, E.E.D. Todd, Q. Zhang, J.-r. Shi, X.-j. Liu, Recent developments in the detection of melamine, Journal of Zhejiang University Science B, 13(2012) 525-32.

[50] P.B. Johnson, R.-W. Christy, Optical constants of the noble metals, Physical review B, 6(1972) 4370.

[51] C. Barrett, K. Dawson, C. O'Mahony, A. O'Riordan, Development of Low Cost Rapid Fabrication of Sharp Polymer Microneedles for In Vivo Glucose Biosensing Applications, ECS Journal of Solid State Science and Technology, 4(2015) S3053-S8.

[52] J.P. Singh, H. Chu, J. Abell, R.A. Tripp, Y. Zhao, Flexible and mechanical strain resistant large area SERS active substrates, Nanoscale, 4(2012) 3410-4.

[53] P. Cahill, N.A.N. Nuallain, N. Jackson, A. Mathewson, R. Karoumi, V. Pakrashi, Energy Harvesting from Train-Induced Response in Bridges, Journal of Bridge Engineering, 19(2014) 04014034.

[54] M.V. Canamares, C. Chenal, R.L. Birke, J.R. Lombardi, DFT, SERS, and Single-Molecule SERS of Crystal Violet, J Phys Chem C, 112(2008) 20295-300.

[55] E.C. Le Ru, E. Blackie, M. Meyer, P.G. Etchegoin, Surface Enhanced Raman Scattering Enhancement Factors: A Comprehensive Study, The Journal of Physical Chemistry C, 111(2007) 13794-803.

[56] S.L. Kleinman, E. Ringe, N. Valley, K.L. Wustholz, E. Phillips, K.A. Scheidt, et al., Single-Molecule Surface-Enhanced Raman Spectroscopy of Crystal Violet Isotopologues: Theory and Experiment, Journal of the American Chemical Society, 133(2011) 4115-22.

[57] R. Chadha, N. Maiti, S. Kapoor, Triplet and SERS study of crystal violet in presence of metal nanoparticles, Chem Phys Lett, 579(2013) 68-72.

[58] L. Angeloni, G. Smulevich, M.P. Marzocchi, Resonance Raman-Spectrum of Crystal Violet, J Raman Spectrosc, 8(1979) 305-10.

[59] Y.J. Kim, X. Sun, J.E. Jones, M. Lin, Q. Yu, H. Li, Surface modification of SERS substrates with plasma-polymerized trimethylsilane nanocoating, Applied Surface Science, 331(2015) 346-52.

[60] K.J. Si, P. Guo, Q. Shi, W. Cheng, Self-Assembled Nanocube-Based Plasmene Nanosheets as Soft Surface-Enhanced Raman Scattering Substrates toward Direct Quantitative Drug Identification on Surfaces, Analytical Chemistry, 87(2015) 5263-9.

[61] M. Vega Canamares, A. Feis, Surface-enhanced Raman spectra of the neonicotinoid pesticide thiacloprid, J Raman Spectrosc, 44(2013) 1126-35.

[62] Y. Zhang, Y. Huang, F. Zhai, R. Du, Y. Liu, K. Lai, Analyses of enrofloxacin, furazolidone and malachite green in fish products with surface-enhanced Raman spectroscopy, Food Chemistry, 135(2012) 845-50.

[63] C. Qiu, A.T. Maingi, C.Y. Jiang, Surface-enhanced Raman scattering detection of melamine via silver nanostructures, Abstr Pap Am Chem S, 241(2011).

[64] S. Söderholm, Y.H. Roos, N. Meinander, M. Hotokka, Raman spectra of fructose and glucose in the amorphous and crystalline states, J Raman Spectrosc, 30(1999) 1009-18.

[65] E.Y.Y. Chan, S.M. Griffiths, C.W. Chan, Public-health risks of melamine in milk products, The Lancet, 372 1444-5.

[66] J.R. Ingelfinger Melamine and the Global Implications of Food Contamination, New England Journal of Medicine, 359(2008) 2745-8.

[67] M. Lin, L. He, J. Awika, L. Yang, D.R. Ledoux, H. Li, et al., Detection of Melamine in Gluten, Chicken Feed, and Processed Foods Using Surface Enhanced Raman Spectroscopy and HPLC, J Food Sci, 73(2008) T129-T34.

[68] E. Koglin, B.J. Kip, R.J. Meier, Adsorption and Displacement of Melamine at the Ag/Electrolyte Interface Probed by Surface-Enhanced Raman Microprobe Spectroscopy, The Journal of Physical Chemistry, 100(1996) 5078-89.

[69] N.E. Mircescu, M. Oltean, V. Chis, N. Leopold, FTIR, FT-Raman, SERS and DFT study on melamine, Vib Spectrosc, 62(2012) 165-71.

[70] S. Yang, J. Ding, J. Zheng, B. Hu, J. Li, H. Chen, et al., Detection of Melamine in Milk Products by Surface Desorption Atmospheric Pressure Chemical Ionization Mass Spectrometry, Analytical Chemistry, 81(2009) 2426-36.

AUTHOR BIOGRAPHIES

Niamh Creedon is studying for a Ph.D. degree at Tyndall National Institute, Cork, Ireland. Her research interests include use of nanomaterials for surface enhanced Raman spectroscopy and electrochemical (bio)sensing.

Pierre Lovera graduated with a diplome d'ingénieur from Phelma in Grenoble and received his PhD from University College Cork in 2009 for his work on optical properties of organic nanowires. He is currently a researcher in the nanotechnology group at Tyndall and his main research interests are in plasmonics, especially surface enhanced Raman spectroscopy, and electrochemistry.

Ambrose Furey received his PhD from Cork Institute of Technology, Ireland. He is currently a senior lecturer in the Department of Physical Sciences, CIT and directs the Mass Spectrometry research group. His current research interests include food safety, security and authenticity and medicinal and pharmaceutical chemical analysis.

Alan O'Riordan received his PhD in 2005, from University College Cork. He is a senior research fellow at the Tyndall National Institute and the principal investigator for smart agri-food and nanosensor systems. His research focuses on using nanomaterials & nanofabrication to develop smart sensor systems, based on Raman spectroscopy and nanoelectrochemistry.

TABLE OF CONTENTS ONLY

Figure Captions:

Fig. 1: (a) Schematic outlining the fabrication of the Ag-covered nanostructured PVDF SERS substrates. (b) Image of Al easily peeling off the templated polymer. (c) Flexible PVDF substrate. (d) SEM image of a PVDF substrate template with the nanostructured Al with 30 nm of Ag deposited over the surface. Inset: Substrate at a higher magnification.

Fig. 2: (a) SEM image obtained from a PVDF substrate coated with 30 nm Ag. (b) 3D geometry constructed by intersecting the parametric surface from the SEM image with blocks using COMSOL (c) FEM simulation showing highly localised electric field enhancements at the metal-dielectric-metal nanogap structures. To avoid possible artifacts at the interface metal/dielectric, the image shows the total electric field at a distance of 2 nm above the surface of the sample

Fig. 3: (a) SERS spectra obtained from 10^{-6} M CV following front excitation on substrates 30 nm Ag (blue) and control experiments in the absence of nanostructure (black) and nanostructured substrates in the absence of CV (green). (b) SERS spectra obtained from 10^{-6} M CV following back excitation on substrates 30 nm Ag (red) and control experiments in the absence of nanostructure (black) and nanostructured substrates in the absence of CV (green). Chart comparing the front and back excitation intensities at peak 1620 cm^{-1} for the control experiments in a and b.

Fig. 4: (a) Waterfall of SERS spectra recorded for 10^{-6} M CV in solution in a single spot over 45 minutes (b) Graph showing the linear relationship between peak area (at 913 cm^{-1}) Vs. droplet drying time.

Fig. 5: (a) SERS spectra recorded for different CV concentrations ranging from 5 x 10^{-10} M to 1 x 10^{-7} M (204 pg/mL –40.8 ng/mL). (b) Graph showing semilog liner relationship between peak area (at 915 cm^{-1}, calculated using a lorentzian function) and concentration of CV (c) 48 separate SERS spectra (10^{-6} M CV concentration) taken at 4 random locations on a single substrate (north south east and west separated by 5 mm) in grids of 10 μm^2 illustrating substrate surface homogeneity. (d) SERS spectra of four representative molecules: imidacloprid, melamine, malachite green and benzocaine.

Fig. 6: (a) Schematic showing partitioning of glucose at a mixed thiol surface and (b) SERS spectra of the mixed monolayer without (black line) and with (dotted line) glucose followed by background subtraction to show a glucose only spectrum (blue).

Fig. 7: SERS spectra of **(a)** 1 ppm melamine spiked in water **(b)** 1 ppm melamine spiked in milk and baby powder, with no pre-treatment

Fig. 8: Mass spectra of melamine standards spiked into (a) deionized water (0.1 ppm) and (b) milk sample (10 ppm), infused into the ESI source (heated) of an Agilent 6340 series ion trap mass spectrometer: (i) M+H+ precursor ion at m/z 127; (ii) MS2 fragmentation of precursor ion at [m/z 127] to yield five predominant characteristic product ions at m/z 109, m/z 97, m/z 84, m/z 85 and m/z 69; (iii) MS3 fragmentation of product ions at m/z 109 to yield the predominant product at m/z 81.

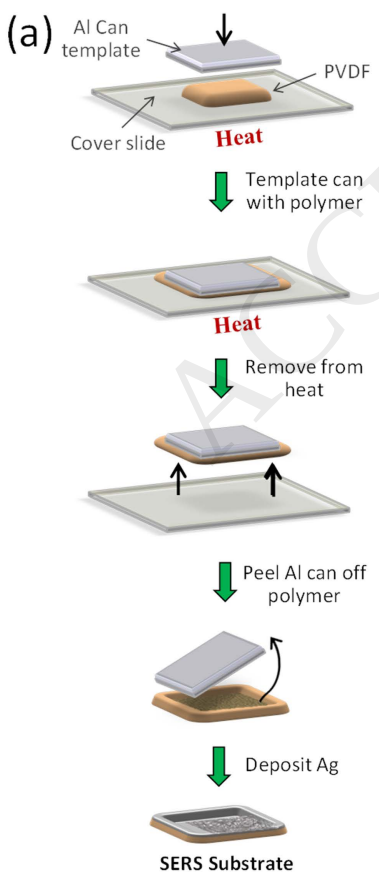
(a)
Al Can template
PVDF
Cover slide
Heat
Template can with polymer
Heat
Remove from heat
Peel Al can off polymer
Deposit Ag
SERS Substrate

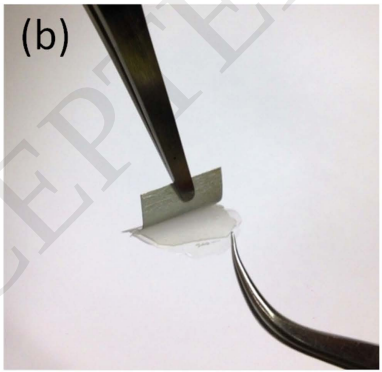
(b)

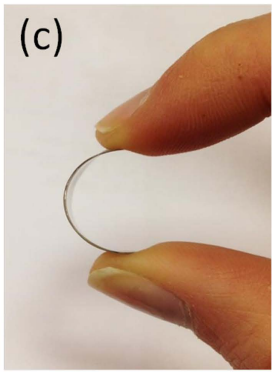
(c)

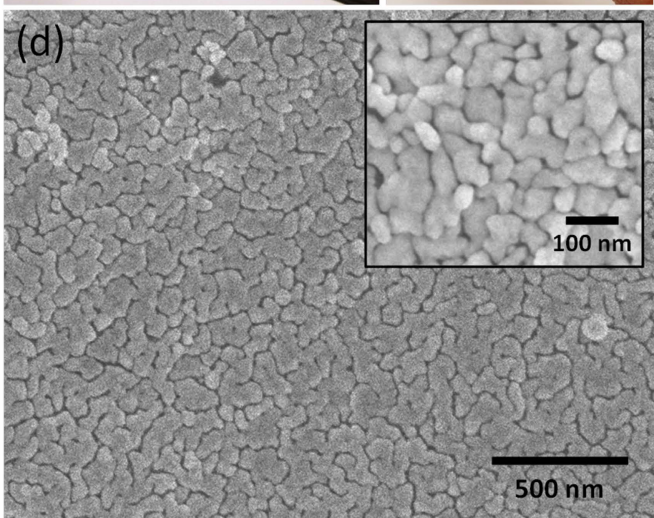
(d)
100 nm
500 nm

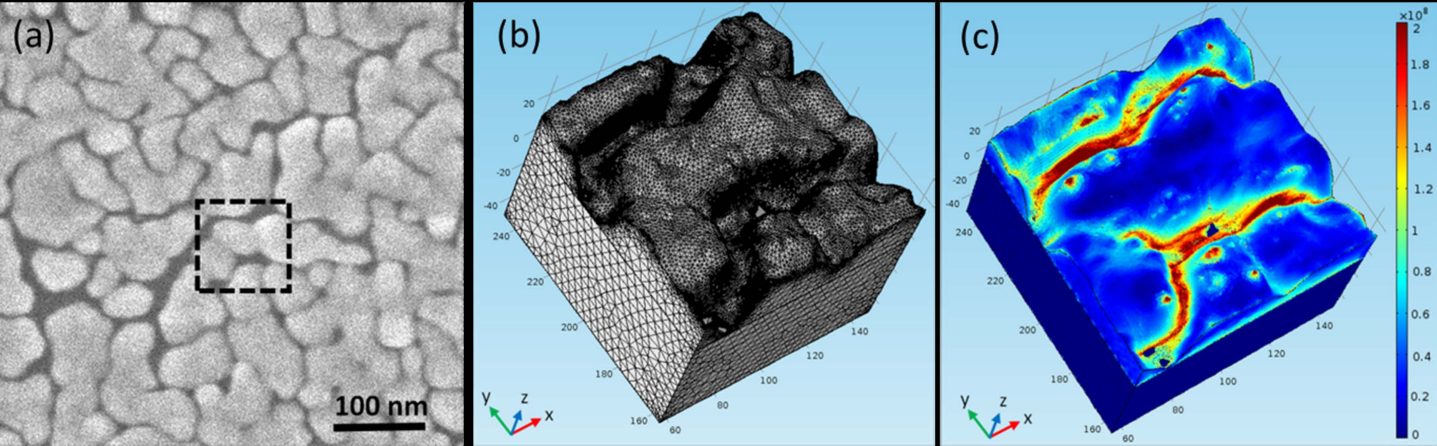
(a)
100 nm
(b)
(c)
×10^8
2
1.8
1.6
1.4
1.2
1
0.8
0.6
0.4
0.2
0
y
z
x

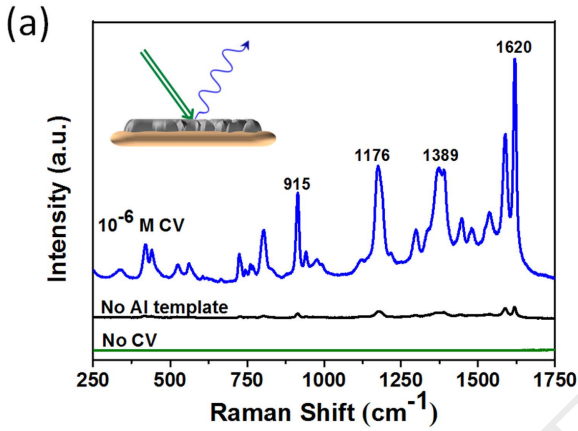
(a)
1620
1176
1389
915
Intensity (a.u.)
10-6 M CV
No Al template
No CV
250
500
750
1000
1250
1500
1750
Raman Shift (cm-1)

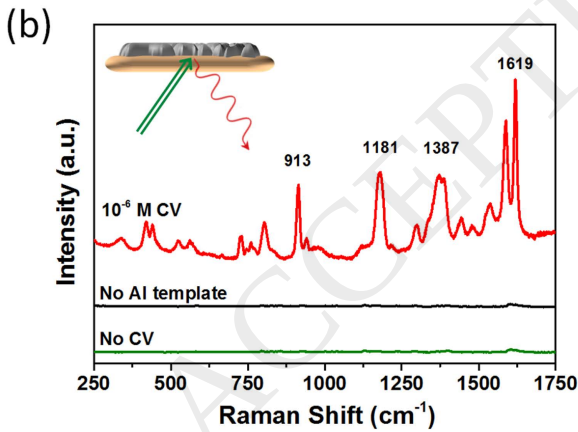
(b)
1619
913
1181
1387
Intensity (a.u.)
10-6 M CV
No Al template
No CV
250
500
750
1000
1250
1500
1750
Raman Shift (cm-1)

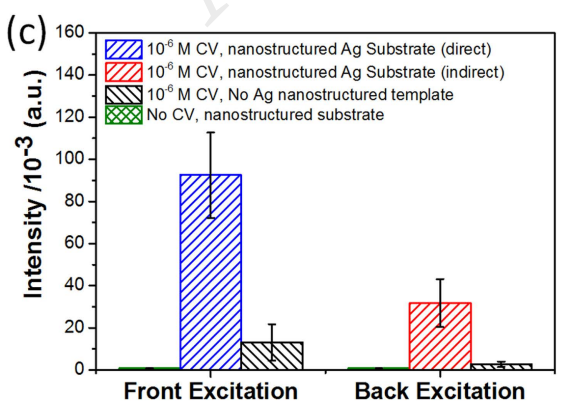
(c)
10-6 M CV, nanostructured Ag Substrate (direct)
10-6 M CV, nanostructured Ag Substrate (indirect)
10-6 M CV, No Ag nanostructured template
No CV, nanostructured substrate
Intensity /10-3 (a.u.)
0
20
40
60
80
100
120
140
160
Front Excitation
Back Excitation

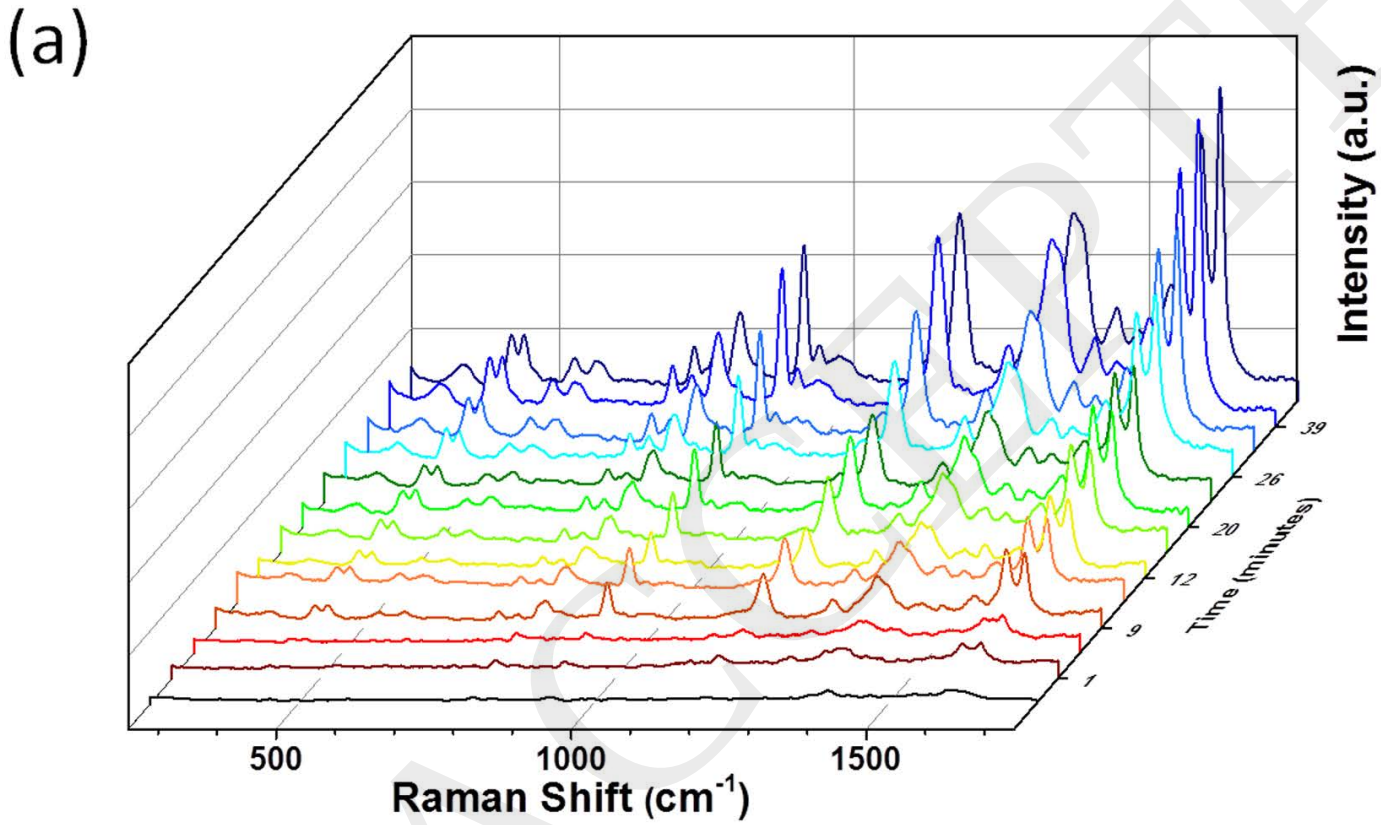
(a)
Intensity (a.u.)
Time (minutes)
39
26
20
12
9
1
500
1000
1500
Raman Shift (cm-1)

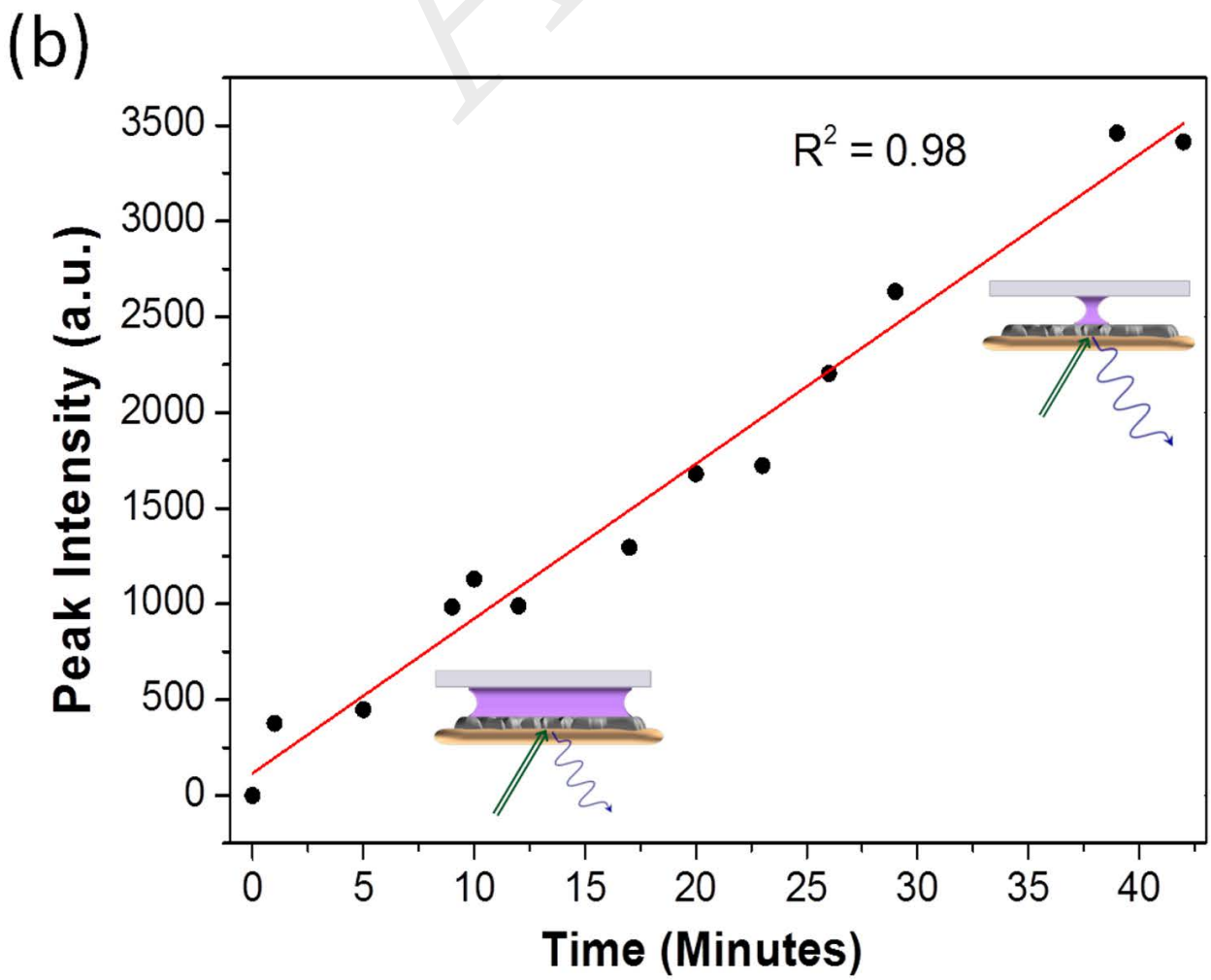
(b)
R2 = 0.98
Peak Intensity (a.u.)
3500
3000
2500
2000
1500
1000
500
0
0
5
10
15
20
25
30
35
40
Time (Minutes)

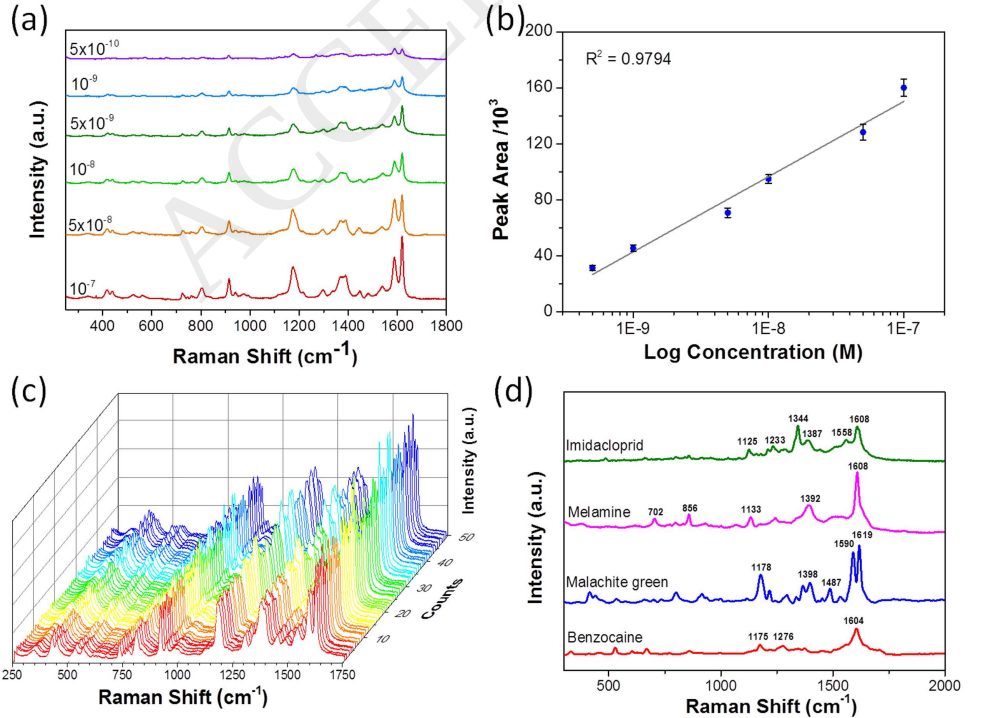
(a)
5x10-10
10-9
5x10-9
10-8
5x10-8
10-7
Intensity (a.u.)
400 600 800 1000 1200 1400 1600 1800
Raman Shift (cm-1)
(b)
R2 = 0.9794
Peak Area /103
0 40 80 120 160 200
1E-9 1E-8 1E-7
Log Concentration (M)
(c)
Intensity (a.u.)
Counts
10 20 30 40 50
250 500 750 1000 1250 1500 1750
Raman Shift (cm-1)
(d)
Imidacloprid
1125 1233 1344 1387 1558 1608
Melamine
702 856 1133 1392 1608
Malachite green
1178 1398 1487 1590 1619
Benzocaine
1175 1276 1604
Intensity (a.u.)
500 1000 1500 2000
Raman Shift (cm-1)

(a)

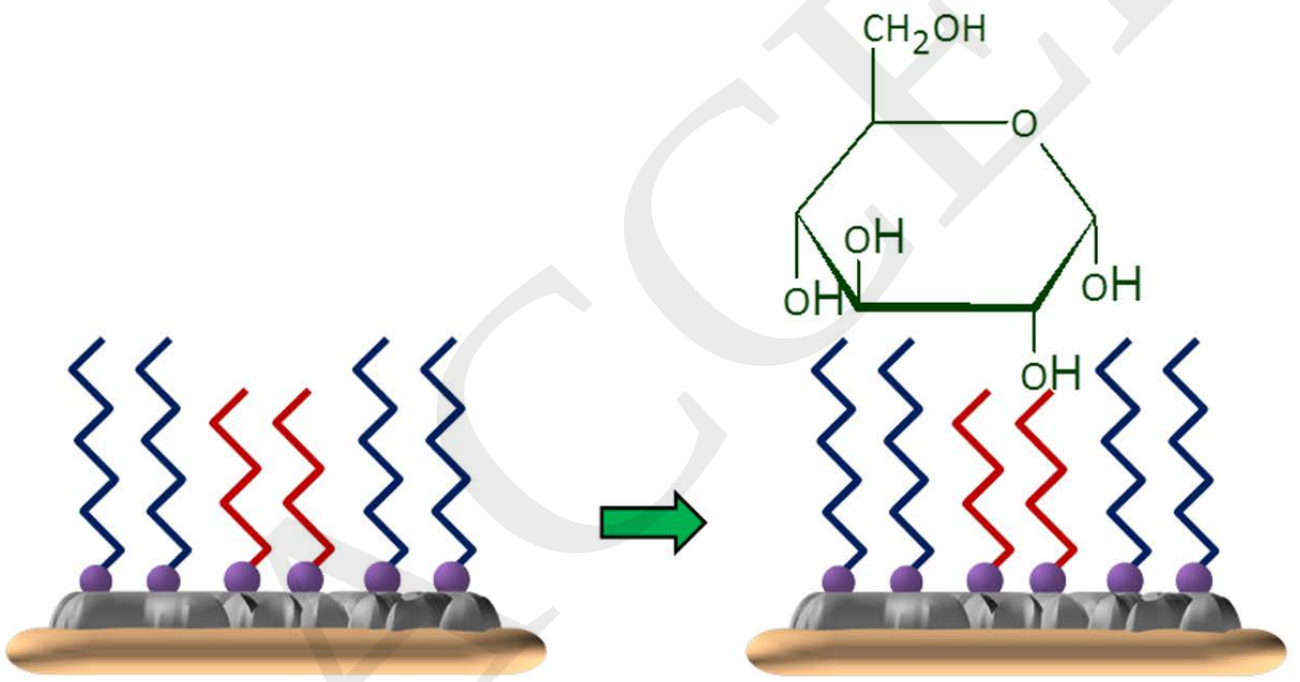
CH2OH
O
OH
OH
OH
OH

(b)

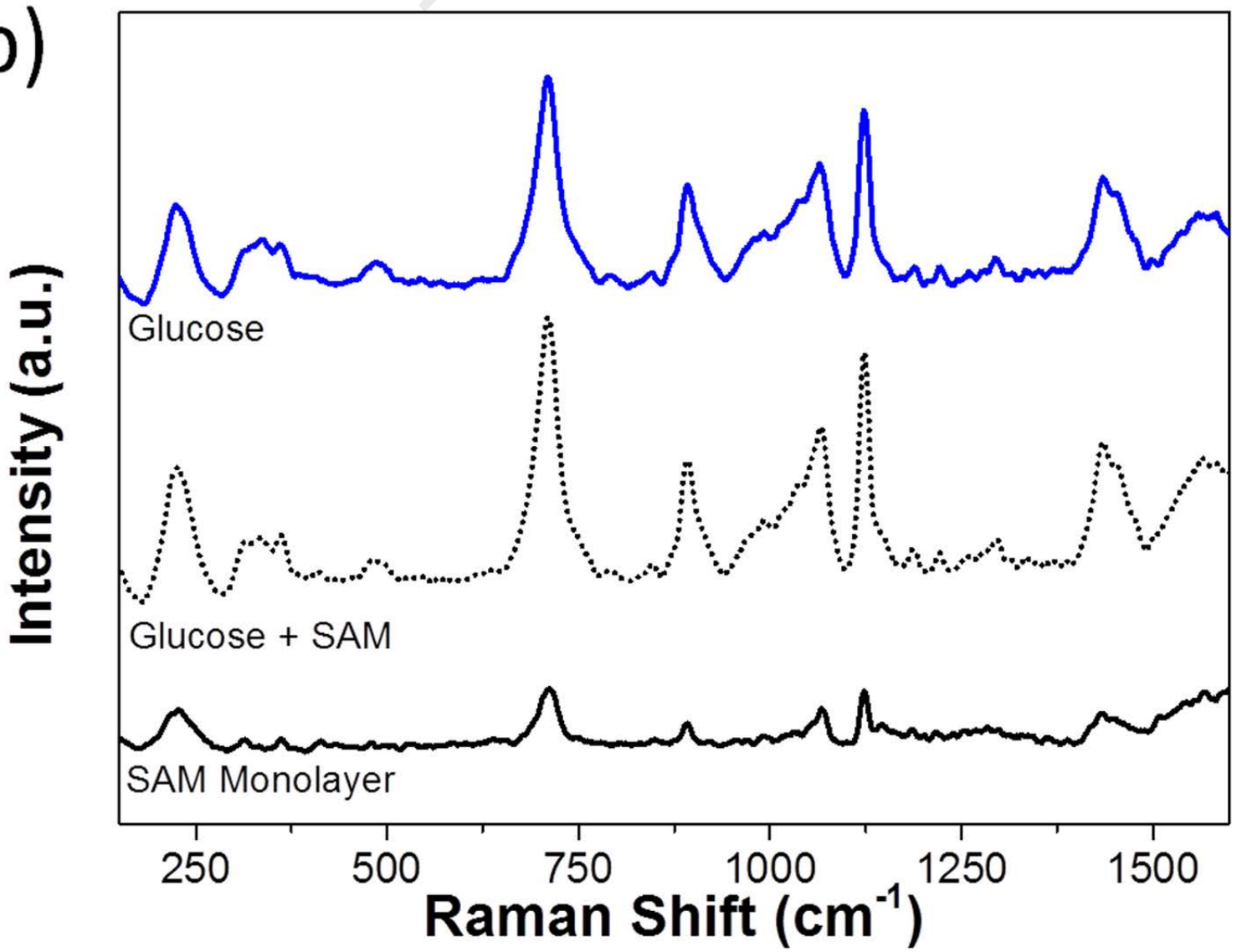
Intensity (a.u.)
Glucose
Glucose + SAM
SAM Monolayer
250
500
750
1000
1250
1500
Raman Shift (cm-1)

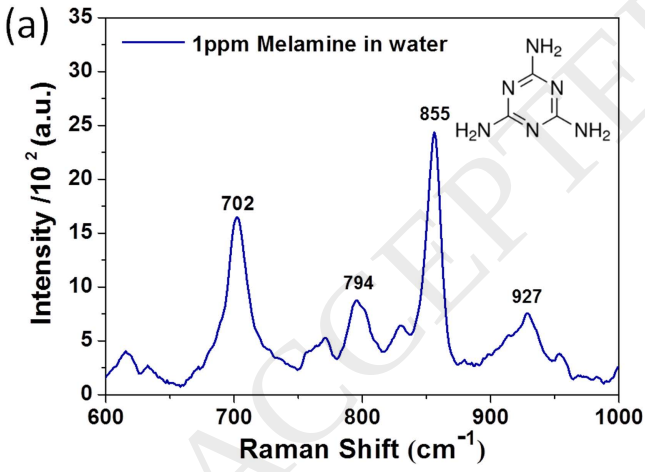
(a)
1ppm Melamine in water
Intensity /10 2 (a.u.)
Raman Shift (cm-1)
702
794
855
927
NH2
N
H2N
(b)
1ppm ML Milk
Milk blank
1ppm ML BF
BF blank
Intensity (a.u.)
701
856
925
702
856
923

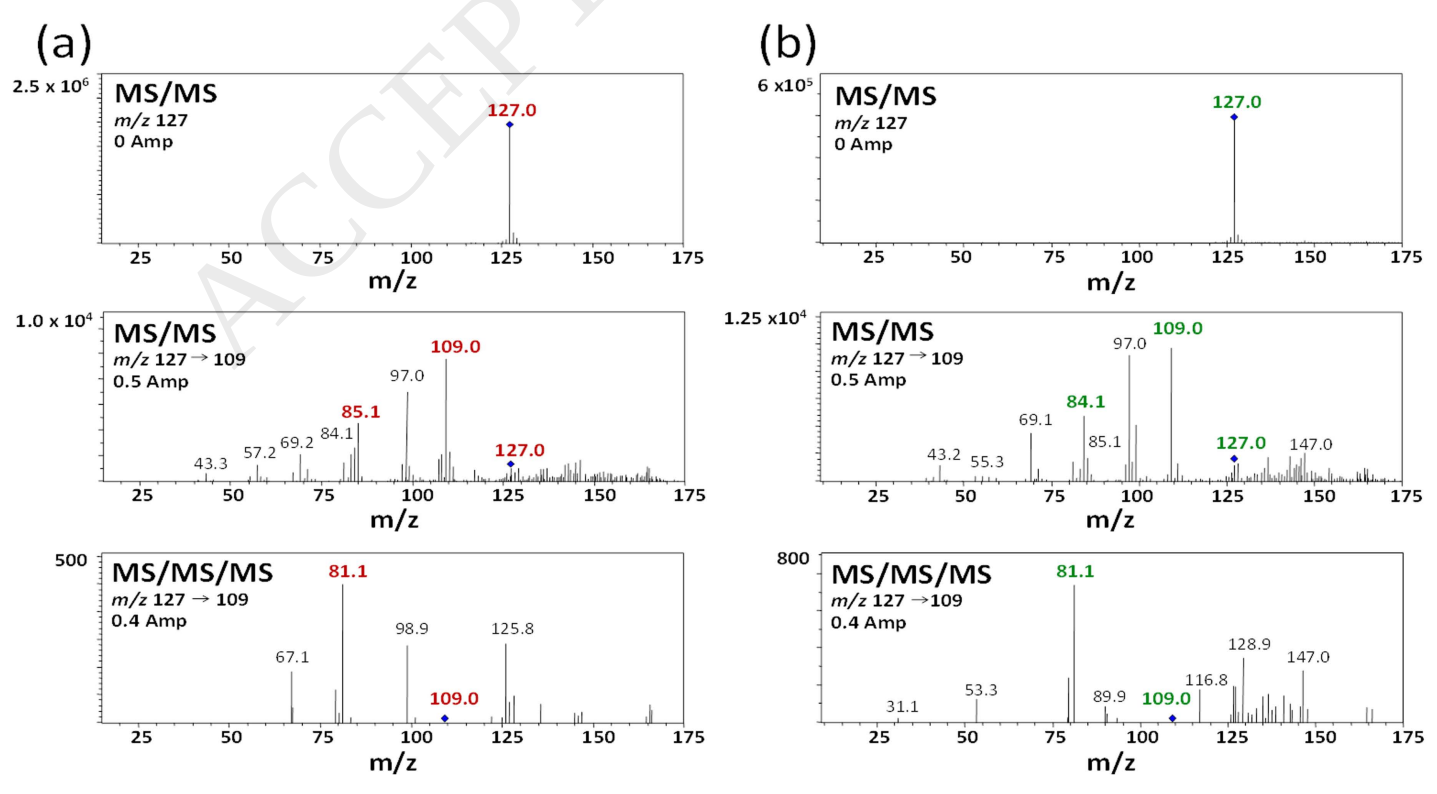
(a)
2.5 x 10^6
MS/MS
m/z 127
0 Amp
127.0
m/z
1.0 x 10^4
MS/MS
m/z 127 → 109
0.5 Amp
109.0
97.0
85.1
84.1
69.2
57.2
43.3
127.0
m/z
500
MS/MS/MS
m/z 127 → 109
0.4 Amp
81.1
98.9
125.8
67.1
109.0
m/z
(b)
6 x10^5
MS/MS
m/z 127
0 Amp
127.0
m/z
1.25 x10^4
MS/MS
m/z 127 → 109
0.5 Amp
109.0
97.0
84.1
69.1
85.1
43.2
55.3
127.0
147.0
m/z
800
MS/MS/MS
m/z 127 → 109
0.4 Amp
81.1
128.9
147.0
116.8
53.3
89.9
109.0
31.1
m/z